Codebook-Based Beamforming Protocols for 5G Millimeter Wave Communications

Pinangkis, Anggrit Dewangkara Yudha; Chandra, Kishor; Prasad, R Venkatesha

Publication date
2018

Document Version
Final published version

Published in
5G Networks

7

Codebook-Based Beamforming Protocols for 5G Millimeter Wave Communications

Anggrit Dewangkara Yudha Pinangkis, Kishor Chandra, and R. Venkatesha Prasad

Electrical Engineering, Mathematics and Computer Science Department, Delft University of Technology, Delft, The Netherlands

7.1 Introduction

The explosive proliferation of mobile devices and ever increasing usage of data-hungry applications have resulted in the need of multi-Gbps wireless access. According to Cisco report [1], in 2015, wired networks still dominated 51% of IP traffic while Wi-Fi and mobile networks accounted for 48%. In 2020, as the number of mobile devices increase, it is predicted that the traffics from Wi-Fi and mobile device will grow significantly and will account for 66% of the global data traffic while the wired networks will only account for 34%. The increasing use of video applications that contribute to 75% of the mobile data traffic is one of the main contributing factors to this unprecedented surge in data traffic. The Next Generation Mobile Networks(NGMN) Alliance has identified several high data rate scenarios for 5G communications such as mass data download from a kiosk, 8K ultra-high definition wireless video transfer, augmented and virtual reality applications, video on demand systems in crowded public spaces, and in-vehicle environments requiring data rates ranging from tens of Mbps to multi-Gbps [2]. Furthermore, the mobile offloading and wireless fronthauling and backhauling would require enormous data rates. For example, extremely high quality (8K) video conferencing and gaming would require a per-user data rate of 300 Mbps in the downlink (DL) and 50 Mbps in the uplink (UL). Considering the mobile broadband access in a highly dense urban environment with 2500 connections/km^2, the resulting DL and UL traffic density would be around 750 Gbps/km^2 and 125 Gbps/km^2, respectively [3]. On the other hand,

5G Networks: Fundamental Requirements, Enabling Technologies, and Operations Management, First Edition. Anwer Al-Dulaimi, Xianbin Wang, and Chih-Lin I.

current 4G system technology, that is, Long Term Evolution (LTE), can only provide a peak data rate of 100 Mbps per user with a DL traffic density 0.77 Gbps/km^2 [4]. Thus, it is evident that a huge gap exists between the future data traffic projections and the capacity of current mobile communication systems. To address this predicted surge in the mobile data usage, 5G networks target a 1000× increase in the existing network capacity [2].

Traditionally, reducing the cell size has been the main driver behind the network capacity growth from 2G to 4G cellular systems. However, the network densification resulting due to the closely spaced small cells in the sub-6 GHz frequency bands is interference limited. Although several techniques of coordinated transmission have been proposed to avoid the interference in small cells, the capacity is still limited by the intercell interference in dense small cell environments. Currently, Wi-Fi (IEEE 802.11b/g/n/ac) operating over 2.4/5 GHz dominates the indoor wireless space. Since its inception, Wi-Fi technology has gone through several amendments to meet the data rate requirements. Despite using very sophisticated physical (PHY) and medium access control (MAC) layer techniques, such as multiple user multiple-input multiple-output (MU-MIMO), higher order modulation and coding, channel bonding and frame aggregation, it is hard to improve the 2.4/5 GHz Wi-Fi data rates any further. For example, the IEEE 802.11ac uses channel bonding and multiuser MIMO schemes but it can only provide a peak data rate of around 1 Gbps because of the limited available bandwidth in the 5 GHz frequency band.

To achieve the targeted 1000× increase in the network capacity, many disruptive approaches are being pursued for 5G communications. These include dense small cell deployment, massive MIMO, millimeter wave (mmWave) radio access and the cloud radio access network (CRAN) architecture, and so on. Millimeter wave frequency band (30–300 GHz) has a large bandwidth availability in both licensed as well as unlicensed bands. This massive available bandwidth can support very high data rates in the order of multi-Gbps. This is why mmWave wireless access has become one of the most preferable air interface for supporting high data rate applications in 5G communications [5–7]. Because of the availability of large bandwidth, radio access and fronthauling and backhauling in the mmWave band (30–300 GHz) has emerged as a key candidate for the multi-Gbps wireless connectivity in the 5G communications [8]. The large frequency chunks are available in 27.5–29.5 GHz, 38.6–40 GHz, 57–66 GHz, 71–86 GHz, and 81–86 GHz bands comprising of both the licensed and unlicensed spectrum (see Figure 7.1). These frequency bands are being investigated for wireless personal area networks (WPANs), wireless local area networks (WLANs), mobile broadband access, and small cell fronthaul and backhaul connectivity in 5G networks. The unlicensed frequency band in 60 GHz band (57–66 GHz) has received most attention for short range high data rate communication resulting in standards such as IEEE 802.15.3c [9] and ECMA-387 [10] for WPAN applications and IEEE 802.11ad [11] for WLAN applications.

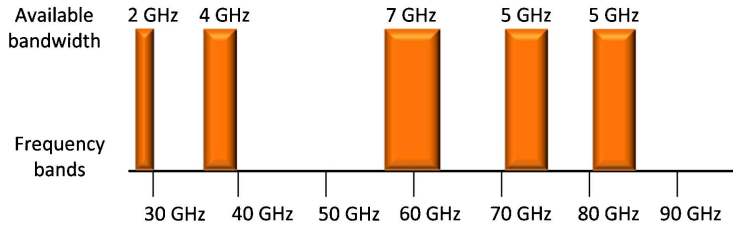

Figure 7.1 Available bandwidths in millimeter wave bands below 90 GHz [8].

The initial standardization efforts such as IEEE 802.15.3c and IEEE 802.11ad in the 60 GHz mmWave bands have mainly focused on WLAN/WPAN operations. However, recent measurement studies have supported the feasibility of mmWave-based mobile communication [12,13]. A further amendment to the 60 GHz WLAN standard IEEE 802.11ad is underway through the recently setup IEEE 802.11ay working group targeting a peak data rate of 20 Gbps using MU-MIMO and channel bonding in unlicensed mmWave bands above 45 GHz. Apart from the WLAN applications, IEEE 802.11ay targets new usage scenarios and applications, including broadband access in crowded public spaces, wireless connectivity in data centers, and fronthaul and backhaul communications in mmWave bands. There are several 5G-PPP projects under the Horizon 2020 Framework Program of the European Commission, such as mmMagic [14], FLEX5GWARE [15], and METIS [16] that are investigating mobile communications at mmWave frequencies.

mmWave-based small cells can provide much needed capacity gain due to the availability of large bandwidth. However, the mmWave signal propagation is significantly different from the sub-6 GHz signal propagations leading to several unique characteristics. As the free-space path loss is proportional to the square of carrier frequency, mmWave signals experience a significantly higher path loss as compared to the 2.4/5 GHz signals. To overcome the path loss, beamforming is used in the mmWave communication [17,18]. Thanks to the short wavelength in mmWave band making it feasible to pack a large number of antenna elements to enable high-gain beamforming. Beamforming results in additional antenna gain to overcome the path loss by focusing the signal power in the desired directions. Apart from the high path loss, an important propagation characteristic of mmWave signals is their limited ability to diffract around obstacles due to the short wavelengths. Furthermore, mmWave signals cannot penetrate through solid materials such as walls and metals. These properties make mmWave links highly susceptible to blockage from obstacles [19]. The highly directional beams that can be steered in the desired direction are much sought in mmWave communications to compensate for the high path loss as well as to circumvent the blockage by obstacles in order to find alternate paths.

Steering high-resolution (narrow beamwidth) beams into the desired direction such that two mmWave devices can communicate with their best beam pair is not easy. Finding the best beam directions can consume a significant amount of allocated channel time, hence, the beamforming technique should be chosen properly. In this chapter, we focus on the beamforming mechanism and protocols that enables fast link setup in mmWave directional links.

In general, there are two kinds of beamforming: adaptive beamforming and switched beamforming. The former depends on the explicit channel estimation that leads to computation and communication overheads, especially in mmWave communications with a large number of antenna elements implementing MIMO [20]. On the other hand, switched beamforming uses fixed predefined antenna sectors and employs MAC layer procedures to find the best beam direction. Antenna sectors are determined using predefined antenna weight vectors (amplitude and phase configurations) that are also called beam codebook. The codebook-based beamforming employs beam searching protocols at MAC layer that find the transmit and receive antenna orientations to find the best beam directions. IEEE 802.15.3c and 802.11ad have adopted codebook-based beamforming employing beam searching protocols at the MAC layer. These beamforming protocols rely on the exhaustive search where a considerable fraction of the allocated time slot is wasted in searching the best direction thus resulting in a very high beam searching overhead. Specially, in the dynamic channel conditions, frequent beam searching would be triggered that will significantly hamper the transmission capacity. Therefore, efficient MAC layer beamforming protocols are required that can find the appropriate beam directions with minimum overhead. Before discussing the beam searching algorithm, we provide a brief introduction of the underlying beamforming architectures as follows.

7.2 Beamforming Architecture

There are three kinds of beamforming architectures, namely, analog beamforming, digital beamforming, and the hybrid beamforming. Each beamforming architecture has its own trade-off between the complexity and the beamforming performance as explained in the following section.

7.2.1 Analog Beamforming

Analog beamforming is the simplest beamforming architecture. This architecture only uses a single radio frequency (RF) chain consisting of an analog to digital converter (ADC) and a mixer (up/down converter), as can be seen in the Figure 7.2. All antenna element weighting factors are applied in the analog domain. Although the analog beamforming is simple, controlling the beam in

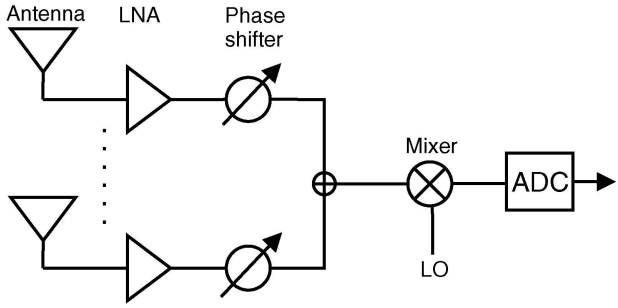

Figure 7.2 Analog beamforming architecture.

analog domain is not flexible. The phase shifts cannot be set to any arbitrary value. As a result, the beam performance (i.e., gain) depends on the resolution of the phase shifters that are attached at each antenna element.

7.2.2 Digital Beamforming

Digital beamforming uses digital signal processor to implement the beamforming algorithm. Since the antenna weighting factors are applied in the digital domain, the phase shift and the amplitude changes can be done flexibly. Each antenna element needs one RF chain that consists of an ADC and an up/down converter, as seen in the Figure 7.3. When a large number of antenna elements are used, the RF chain consumes a lot of power and it also increases the system cost.

7.2.3 Hybrid Beamforming

Hybrid beamforming can leverage the benefits of both analog and digital beamforming. It offers performance close to digital beamforming but with less num-

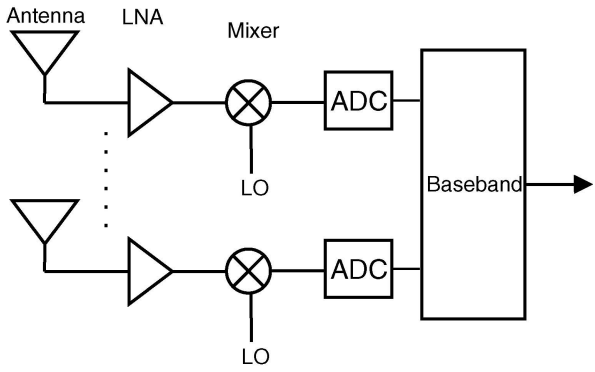

Figure 7.3 Digital beamforming architecture.

ber of RF chains. Hybrid beamforming can be roughly divided into two categories, namely, fully connected and partially connected, as shown in Figure 7.4, where N_{RF} RF chains serve M antenna elements. In fully connected architecture, each RF chain is connected to all antennas while in partially connected systems, each RF chain is connected to a set of antenna elements. A fully connected beamforming system requires $M \times N_{RF}$ analog phase shifters while a partially connected system requires M analog phase shifters. Consequently, a fully connected architecture provides N_{RF} times higher beamforming gain per transceiver than the partially connected system.

Due to its ability to reduce the number of RF chains, hybrid beamforming has emerged as a preferable solution in the 5G mmWave communications that exploits MIMO technology [21,22]. In particular, it is highly suitable for the beamforming employing massive MIMO technology where antenna arrays would consist of hundreds of antenna elements [23].

Hybrid beamforming approaches the ideal codebook (w) by multiplying predefined RF codebook (w_{RF}) and predefined baseband codebook (w_{BB}). In this case, w_{RF} is restricted by the set of feasible RF codebook $w_{RF_{dict}}$. Minimizing RMSE in $||w - w_{RF}w_{BB}||_2$ means that the beam in the hybrid architecture will be closer to the one in the fully digital architecture.

$$\begin{aligned}(w_{RF}^{opt}, w_{BB}^{opt}) &= \underset{w_{RF}, w_{BB}}{\arg\min} \| \, w - w_{RF}w_{BB} \, \|_2 \\ &\text{s.t.}[w_{RF}] \, \epsilon \, w_{RF_{dict}} \\ &\| \, w_{RF}w_{BB} \, \|_2^2 = 1.\end{aligned} \tag{7.1}$$

There are some proposed algorithms to minimize the difference between the fully digital codebook and the hybrid codebook. To find the solution of Eq. 7.1, References [24] and [25] employ orthogonal matching pursuit (OMP) algorithm. In Reference [26], orthogonal matching pursuit with dynamic dictionary learning (DDL–OMP) algorithm, which is a modified version of OMP algorithm, is used to solve the problem. A geometric approach algorithm is also proposed in Reference [27]. Beams created in OMP algorithm, DDL–OMP algorithm, and geometric approach algorithm compared with fully digital beamforming are shown in Figure 7.5. The performance comparison of three algorithm in the hybrid beamforming is shown in the Figure 7.6. It can be seen that the geometric approach algorithm outperforms both OMP algorithm and DDL–OMP algorithm.

7.3 Beam Searching Algorithm

Unlike adaptive beamforming where the best beam direction is defined by measuring full channel state information (CSI), beam searching in the switched

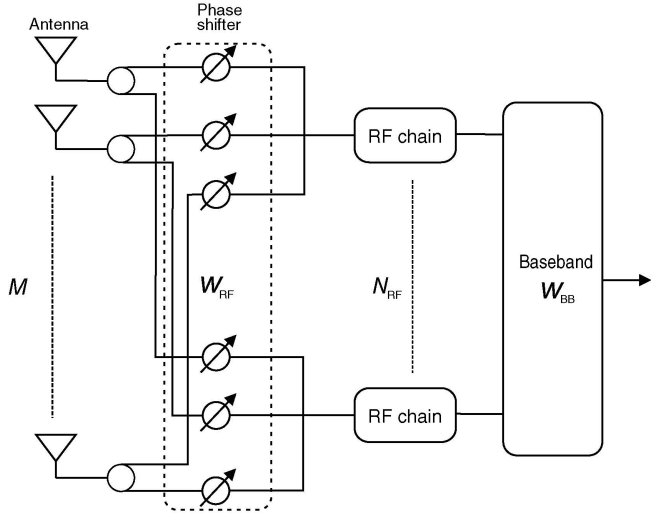

(a) Fully connected hybrid beam forming.

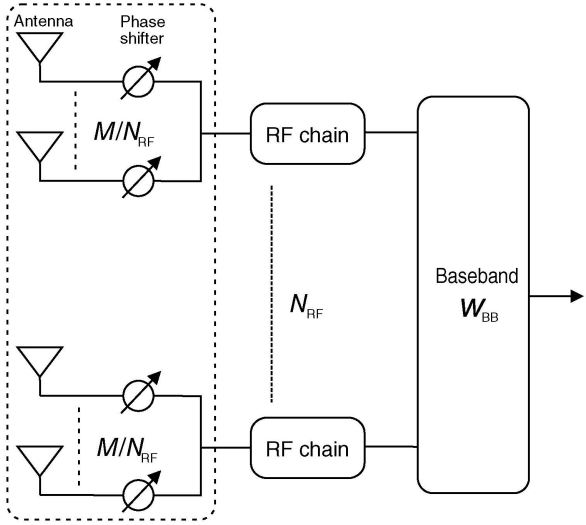

(b) Partially connected hybrid beam forming.

Figure 7.4 Hybrid beamforming architectures.

beamforming only depends on the measured signal quality of each predefined beams. Transmitter and receiver devices exchange their training packet to measure the channel quality for each beam candidate. Nevertheless, finding the best beam pair in the mmWave communication that exploits very narrow

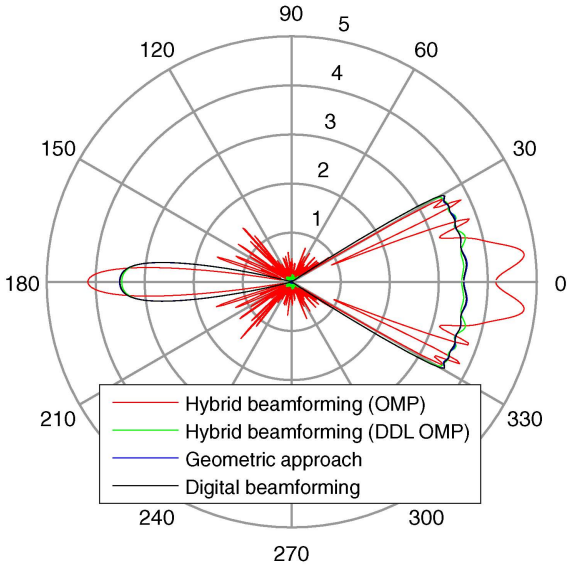

Figure 7.5 Beam patterns based on FSM-KW. The beams are created with 128 antenna elements in fully digital beamforming, hybrid beamforming with 8 RF chains using OMP algorithm, and hybrid beamforming with 8 RF chains using DDL OMP algorithm.

beamwidth is not easy. As the number of beams rises or the beam resolution gets higher, the number of training packets also increase.

7.3.1 IEEE 802.15.3c Beam Searching

IEEE 802.15.3c is a standard for wireless personal access networks (WPANs) for high data rate in 60 GHz [28,29]. This standard is based on piconet network that organizes communication between devices (DEVs) through piconet controller (PNC). PNC is a DEV that has the capability to control the network.

The PNC will start transmitting beacon using its quasiomni level beam to identify DEVs around the PNC that want to join the network before starting the beamforming. There are two level beam searching in the beamforming. The first level is sector level that is considered as a coarse level. The sector level beam is needed to find the area of interest and to find the best sectors for both DEVs. It will be followed by beam level where some beams will be covered by one sector. The beam level will select the best pair beams covered in the best selected sector. The beam searching, both in sector level and beam level, will be done in brute force search. Therefore, the number of training packets will be

$$N = \alpha(N_1^{\mathrm{s}} \times N_2^{\mathrm{s}} + N_1^{\mathrm{b}} \times N_2^{\mathrm{b}}), \tag{7.2}$$

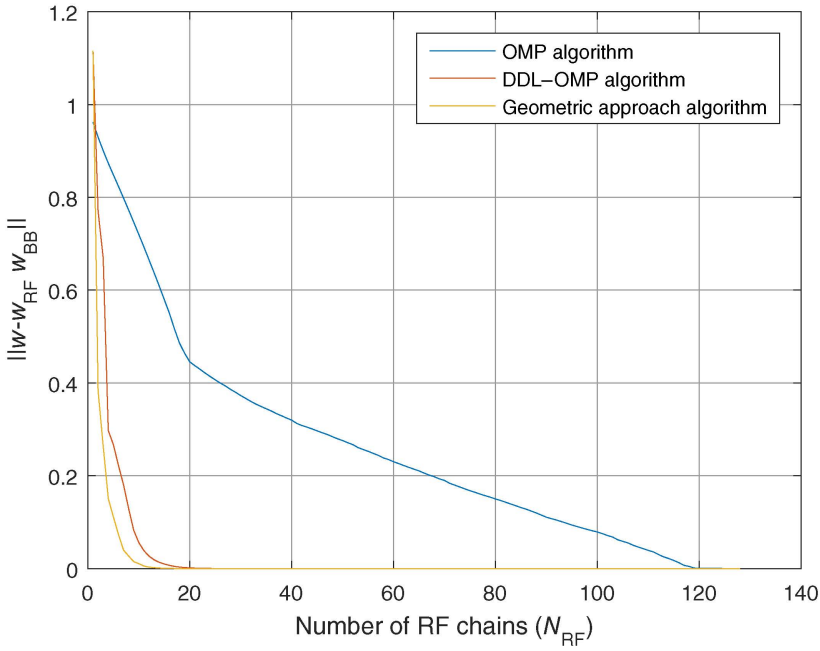

Figure 7.6 Comparison of root mean square error (RMSE), $||w - w_{\mathrm{RF}} w_{\mathrm{BB}}||_2$, with various number of RF chains in OMP algorithm, DDL–OMP algorithm and geometric approach algorithm. In this case, the beam created is based on FSM-KW beamforming, $A = 40$ and $M = 128$.

where $\alpha = 1$ when the channel is symmetrical and $\alpha = 2$ when the channel is asymmetrical. N_1^{s} and N_2^{s} denote number of sector candidates in DEV1 and DEV2, respectively, while N_1^{b} and N_2^{b} denote the number of beams covered by one sector in DEV1 and DEV2, respectively.

7.3.2 IEEE 802.11.ad Beam Searching

Instead of calling the device as DEV as in IEEE 802.15.3c, IEEE 802.11ad calls the device as station or STA. Before starting beamforming, STA1 will transmit beacons to initiate communication with STA2. The beacons are transmitted through its quasiomni beam (Figure 7.7).

Similar to IEEE 802.15.3c, IEEE 802.11ad also exploits two level of beam-training mechanism [30]. However, instead of using exhaustive beam searching at each level of beam searching as in IEEE 802.153c, IEEE 802.11ad uses its best sector or its best beam to receive the training packets. The beam-training mechanism is shown in Figure 7.8. By doing sector level beamforming and beam level beamforming, the total training packets will be

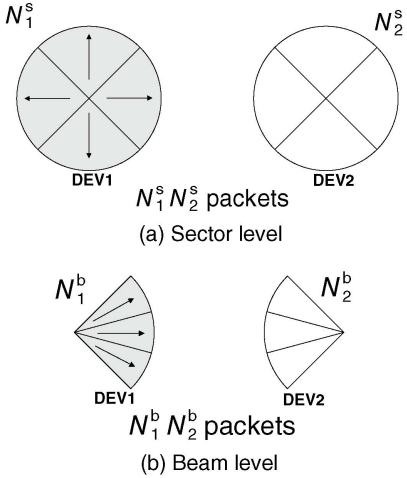

Figure 7.7 Beamforming mechanism in IEEE 802.15.3c (symmetrical channel condition).

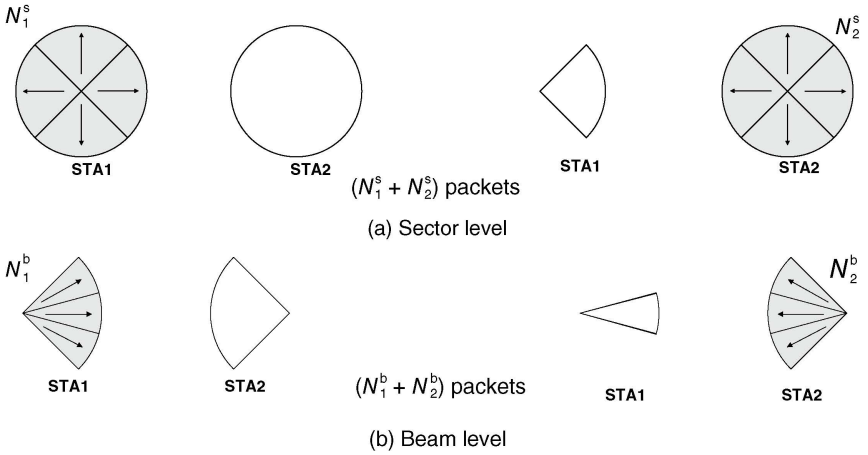

Figure 7.8 Beam searching mechanism in IEEE 802.11ad (symmetrical channel condition).

$$N = \alpha(N_1^s \times N_2^s + N_1^b \times N_2^b), \tag{7.3}$$

where $\alpha = 1$ when the channel is symmetrical and $\alpha = 2$ when the channel is asymmetrical. N_1^s and N_2^s represent the number of sectors in STA1 and STA2, respectively. N_1^b and N_2^b represent the number of beams covered by one sectors in STA1 and STA2, respectively.

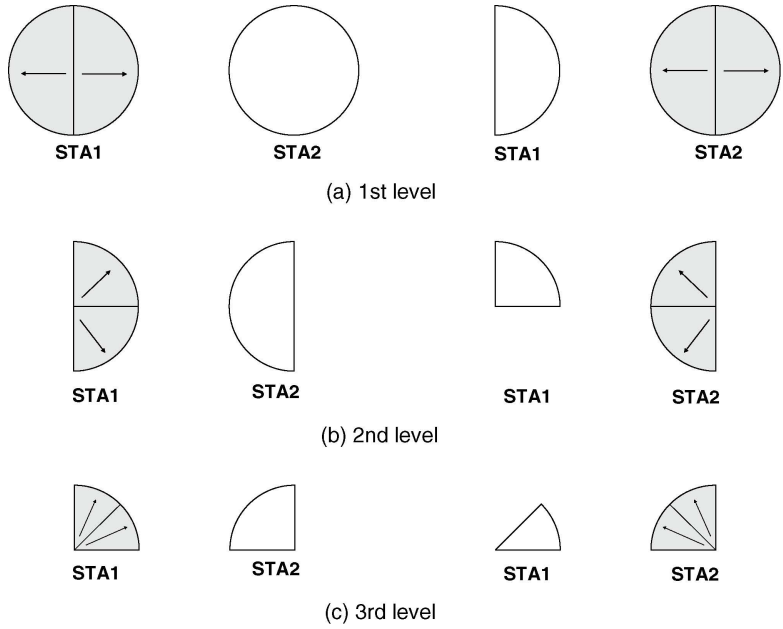

Figure 7.9 Illustration of beam searching mechanism in decrease-and-conquer (symmetrical channel condition).

7.3.3 Hierarchical Beam Searching

Instead of using only two-level beam searching as proposed in IEEE 802.15.3c and IEEE 802.11ad, hierarchical beam searching consists of multilevels. Hierarchical beam searching is proposed in References [26,31–35]. In order to minimize the beam training overhead, hierarchical beamforming generally uses two beam candidates at each level as can be seen in Figure 7.9. Therefore, the searching will follow a binary search-like algorithm.

By doing binary search-like beam searching, the total number of training packets will be

$$N = \alpha(2\log_2 N_1 + 2\log_2 N_2), \tag{7.4}$$

where N_1 is the number of possible finest beams in STA1, N_2 is the number of possible finest beams in STA2, $\alpha = 1$ when the channel is symmetrical and $\alpha = 2$ when the channel is asymmetrical. If N_1 and N_2 is associated with N_1^{s}, N_1^{b}, N_2^{s} and N_2^{b} as in IEEE 802.15.3c and IEEE 802.11ad, they will be equivalent with $N_1 = N_1^{\mathrm{s}} \times N_1^{\mathrm{b}}$ and $N_2 = N_2^{\mathrm{s}} \times N_2^{\mathrm{b}}$.

7.4 Codebook Design

Switched beamforming requires predefined codebook so that the beam candidates can be generated directly from the codebook. Codebook that consists of K beam candidates and M number of antenna elements is a $M \times K$ matrix that represents amplitude and phase shift changes at each antenna element. By adjusting the signal at each antenna element, the beam can be steered at a specific direction.

$$w = \begin{bmatrix} w_{1,1} & w_{1,2} & \dots & w_{1,K} \\ w_{2,1} & w_{2,2} & \dots & w_{2,K} \\ \dots & \dots & \dots & \dots \\ w_{M,1} & w_{M,2} & \dots & w_{M,K} \end{bmatrix} \tag{7.5}$$

7.4.1 IEEE 802.15.3c Codebook

Codebook is defined specifically in IEEE 802.15.3c, but there is no specific codebook defined in IEEE 802.11ad. In order to reduce the complexity, IEEE 802.15.3c standard only uses limited phase shift adjustment without amplitude changes. The phase shift is limited to 2-bit of resolution or $0, \pi/2, \pi, 3\pi/2$ [28].

When the number of possible beams is more than the number of antenna elements, $K > M$, the codebook is defined as

$$w(m,k) = j^{\text{fix}\{\frac{m \times \text{mod}[k+(K/2),K]}{K/4}\}} \quad \text{for} \quad m = 0 : M-1 \text{ and } k = 0 : K-1, \tag{7.6}$$

for a special case when $K = M/2$

$$w(m,k) = \begin{cases} (-j)^{\text{mod}(m,k)}, & \text{for} \quad m = 0 : M-1 \text{ and } k = 0 \\ (-1)^{\text{fix}\{\frac{mx \times \text{mod}[k+(K/2),K]}{K/4}\}} & \text{for} \quad m = 0 : M-1 \text{ and } k = 1 : K-1 \end{cases} \tag{7.7}$$

Beam candidates with $M = 2$ $K = 4$ and $M = 4$ $K = 8$ are shown in Figure 7.10. It can be seen that due to limited phase shifter resolution, some beams cannot reach maximum gain. Moreover, there is a gap between adjacent beams that can be counted as loss. Therefore, to reduce the cusp loss, the number of antenna elements is set equal to twice the possible beams [36].

7.4.2 N-Phase Beamforming

N-phase beamforming is similar to IEEE 802.15.3c. However, this beamforming is designed to accommodate the availability of higher phase shift resolution.

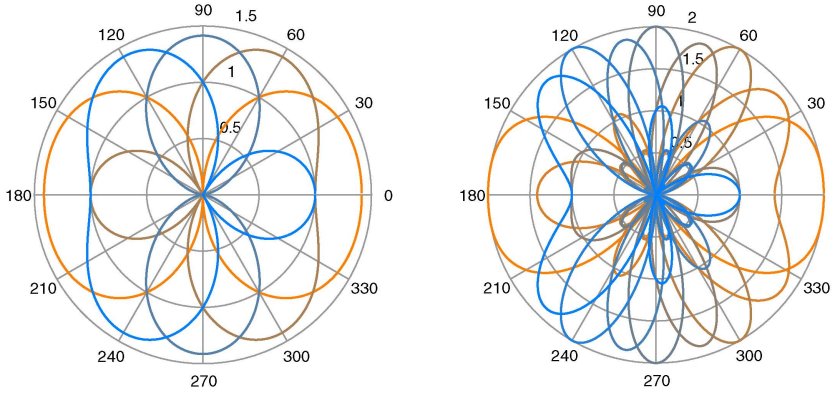

(a) K= 4 and M= 2 (b) K= 8 and M= 4

Figure 7.10 IEEE 802.15.3c beamforming with various number of beams.

Instead of using only 4-phase or 2-bits of resolution, this beamforming uses N-phase [37]. The codebook is defined as

$$w(m,k) = j^{\frac{2\pi}{N}\text{fix}\{\frac{m\times\text{mod}[k+(K/2),K]}{K/N}\}} \quad \text{for} \quad m = 0:M-1 \text{ and } k = 0:K-1, \tag{7.8}$$

where M is number of antenna elements and K is number of possible beams.

Since the phase shifter resolution is higher than the one in IEEE 802.15.3c codebook, this beamforming offers better beamforming as depicted in Figure 7.11 where eight beams are generated with $N = 4$. All the beam candidates can reach maximum gain, unlike in IEEE 802.15.3c where some beams have lower array factor than the others. Nevertheless, for higher beam resolution higher phase resolution is needed.

7.4.3 DFT-Based Beamforming

Digital Fourier Transmorm (DFT)-based beamforming gives more flexible beams where each beam can reach the same maximum gain. However, this beamforming requires more flexible phase shift to compensate the flexibility of the beams.

DFT-based codebook can be formulated as

$$w(m,k) = \text{e}^{-j2\pi mk/K} \quad \text{for} \quad m = 0:M-1 \text{ and } k = 0:K-1, \tag{7.9}$$

where M is number of antenna elements and K is number of possible beams (Figure 7.12).

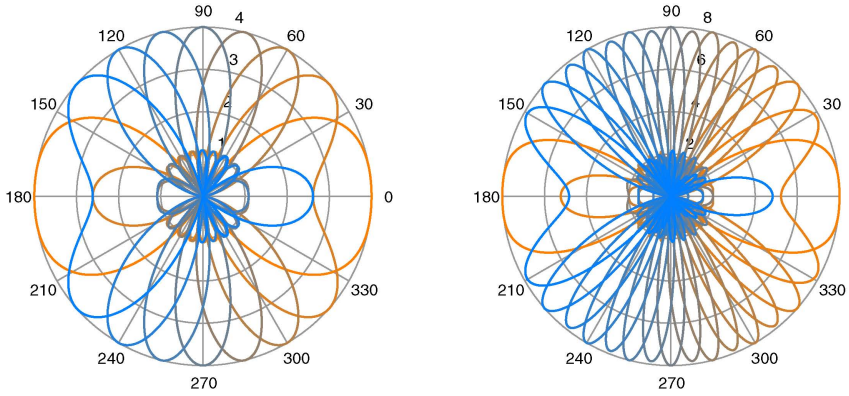

(a) $K = 8$ and $M = 4$ (b) $K = 16$ and $M = 8$

Figure 7.11 N-phase beamforming with N=8 and various number of beams generated.

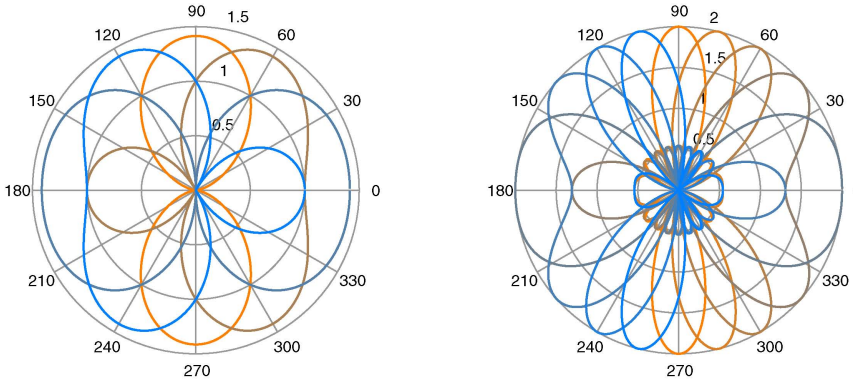

(a) $K = 4$ and $M = 2$ (b) $K = 8$ and $M = 4$

Figure 7.12 DFT-based beamforming with various number of beams.

From Eq. 7.9, it can be seen that the codebook requires higher phase shift resolution as K increases. The phase shift resolution in this codebook is $b = \log_2(K)$.

Compared to IEEE 802.15.3c, with the cost of higher phase shift resolution DFT-based codebook gives better beamforming performance where all of its possible beams can reach maximum gain. Beamforming in IEEE 802.15.3c when $K = 32$ suffers cusp loss 1.98 dB or losing about 36% of its power. If this beamforming is used in both DEV1 and DEV2, it is potential to loose 3.96 dB or 60% of its power. It can be seen that DFT codebook can minimize the losses where there is only 0.91 dB of loss. However, if both DEV1 and DEV2 suffers

maximum cusp loss, it still have 1.92 dB of losses or about 35% of its power in total.

7.4.4 Fourier Series Method with Kaiser Window (FSM-KW) Beamforming

FSM-KW beamforming can be seen as a bandpass filter in the angle space domain [38]. This beamforming is intended to have uniform array factor in the desired beamwidth. Kaiser window is chosen in Reference [26] since the trade-off between sidelobe attenuation and beam transition width can be adjusted.

Beamforming codebook in FSM-KW can be defined as

$$w(m) = w_{\text{window}}(m)\mathrm{e}^{-i\beta\psi_o}\frac{\sin(\beta\psi_b)}{\pi\beta} \text{ for } m = 0, 1, ..., M-1, \tag{7.10}$$

where $w_{\text{window}}(m)$ are the Kaiser window samples and $\beta = m - M/2$ while ψ_o and ψ_b are given as

$$\psi_o = \frac{\pi}{2}(\cos\theta_1 + \cos\theta_2), \tag{7.11}$$

$$\psi_b = \pi\sin(\theta_c)\sin\left(\frac{\Delta\theta}{2}\right) + \frac{\pi D}{M-1}. \tag{7.12}$$

The D-factor can be defined from the sidelobe attenuation A (dB)

$$D = \begin{cases} \frac{A-7.95}{14.36}, & \text{if} \quad A > 21 \\ 0.922, & \text{if} \quad A \leq 21. \end{cases} \tag{7.13}$$

The γ factor can be calculated as

$$\gamma = \begin{cases} 0.11(A-8.7), & \text{if} \quad A \geqslant 50 \\ 0.58(A-21)^{0.4} + 0.079(A-21), & \text{if} \quad 21 < A < 5 \\ 0, & \text{if} \quad A \leq 21. \end{cases} \tag{7.14}$$

The Kaiser window samples itself are given as

$$w_{\text{window}}(m) = \frac{I_{\text{o}}(\gamma\sqrt{1-4\beta^2})}{I_{0\times 2}(\gamma),} \tag{7.15}$$

where I_0 is the zeroth order modified Bessel function of the first kind.

Unlike the IEEE 802.15.3c beamforming, N-phase beamforming, DFT-based beamforming, and FSM-KW beamforming can generate almost uniform array factor in the desired beamwidth with only small fraction of beamforming. Since the beamwidth and the beam direction can be set flexibly, this beamforming can be used in the hierarchical beam searching algorithm where the beam searching

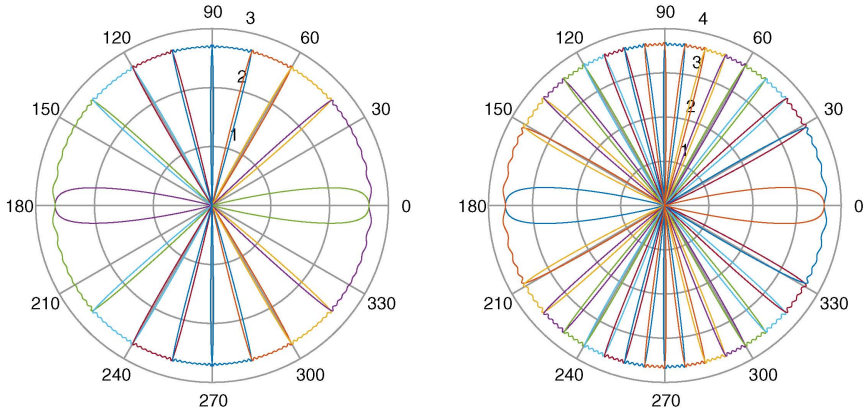

(a) $K = 8$ and $M = 128$ (b) $K = 16$ and $M = 128$

Figure 7.13 Beamforming based on FSM-KW beamforming that is used in Reference [26] and implemented on fully digital beamforming.

area can be divided into two areas at each beam searching level. The resulting beams using the FSM-KW beamforming can be seen in Figure 7.13.

7.5 Beamforming Evaluation

Comparing the three beam searching algorithms mentioned in Section 7.3, hierarchical beam searching has the lowest number of training packets if the hierarchical process is done in binary-like search. The comparison of training packets for some arbitrary number of beams is shown in Table 7.1. It can be concluded that hierarchical beam searching performance is better than the other mentioned beam searching methods.

Discussing how to design the beams, FSM-KW beamforming can accommodate hierarchical beam searching with low beam intersection and almost flat array factor in the 360° coverage. Although it costs more antenna elements compared to other beamforming, the complexity can be reduced with hybrid beamforming. Moreover, hybrid beamforming also offers ability to generate multiple beams that will be useful in the MIMO system.

Nevertheless, in general codebook design in IEEE 802.15.3c standard N-phase beamforming, and DFT-based beamforming, FSM-KW beamforming do not take into account the beam pattern of element antenna. The element pattern is assumed to have an isotropic beamforming that has the same gain in all angle direction. Therefore, the beam pattern is assumed to be the same as the array factor in the array antenna.

Table 7.1 Illustration of comparison of training packets in IEEE 802.15.3c, IEEE 802.11ad, and decrease-and-conquer beamforming, taking assumption that the channel is symmetric and both devices have the same number of sectors and beams.

Number of Sectors	Number of Beams per Sector	Number of Training Packets (Symmetrical Channel)		
		IEEE 802.15.3c	IEEE 802.11ad	Hierarchical (2 Beam Candidates)
4	2	20	12	12
4	4	32	16	16
8	8	128	32	24
8	16	320	48	28

In reality, it is impractical to steer the beam at low angle direction. A patch antenna that is usually used as an antenna element in the array antenna has limited beamwidth that will lead to scanning angle limitation, which is usually until $\pm 60^{o}$ from the broadside direction [39,40]. Beamforming in more realistic condition when considering that a patch antenna has sinusoid beam pattern, $E(\theta) = \sin(\theta)$, as shown in Figure 7.14.

A patch antenna is usually preferred as an array antenna component due to its compactness, for example, patch antenna designed in Reference [41] has size of 1.7 mm × 2 mm. If this factor is not being considered such that 360^{o} is only covered with one array antenna system, the beam at low-angle direction will have very low gain. Therefore, it is suggested to limit the beamforming scanning angle $\pm 60^{o}$ from the broadside direction so that there are at least three antenna system to cover 360^{o}.

7.6 Conclusion

In the context of 5G, mmWave communication has established itself as the main candidate for the multi-Gbps wireless connectivity in WPAN/WLANs and cellular access, backhaul and fronthaul in dense small cells. The small wavelength of mmWave signals allows close packing of a large number of antenna elements to form highly directional antenna arrays that can compensate for the high path loss observed at mmWave frequencies. However, forming a mmWave link using narrow beams is not easy as the receive and transmit antenna arrays need to find each other. The time spent to find the best beam directions has a direct consequence on the medium access utilization [42] as well as the initial access procedures [43] to discover an access point or base station. Generally, beamforming is performed using two approaches, namely, adaptive beamforming and switched beamforming. Switched beamforming outperforms adaptive

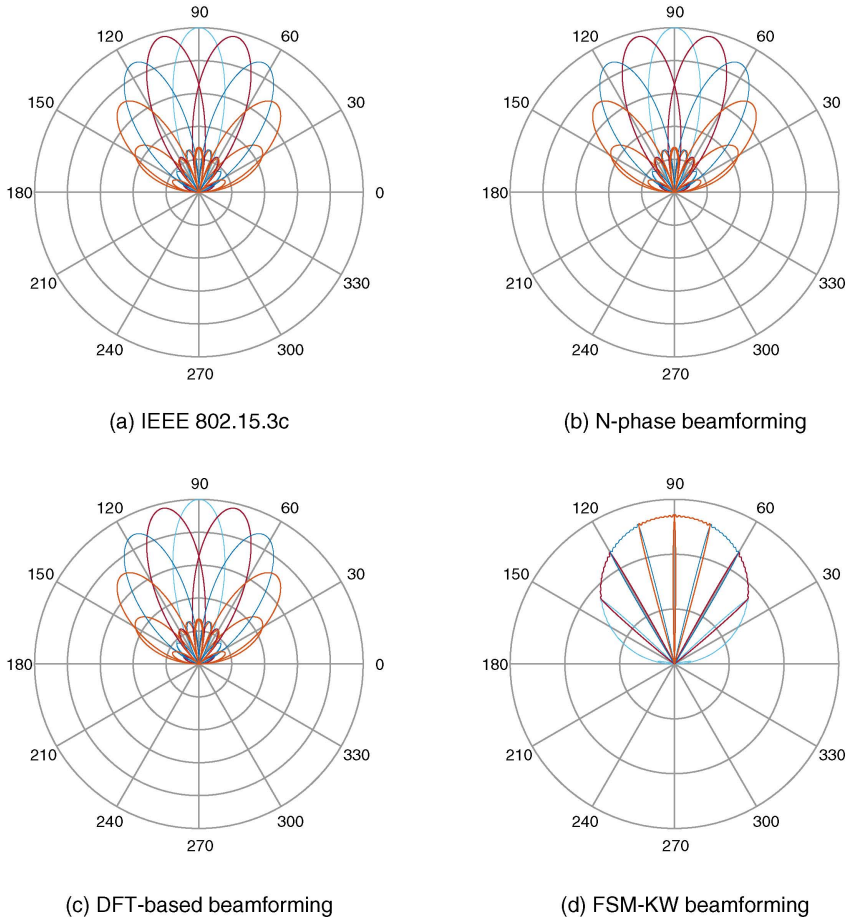

Figure 7.14 Field pattern of beamforming in (a) IEEE 802.15.3c, (b) N-phase, (c) DFT based, and (d) FSM-KW when the antenna element pattern is considered (taking assumption $E(\theta) = \sin(\theta)$).

beamforming in terms of computational complexity that has a direct impact on the baseband power consumption that is an important factor at mmWave frequencies. However, switched beamforming has limited flexibility where the beams have discrete angle directions. The discretization of beam directions introduces intersection loss (cusp loss) between the adjacent beam candidates. A compromising approach called hybrid beamforming that uses both the digital and analog beamforming has emerged as an attractive alternative to realize the mmWave beamforming. It is power efficient than the digital beamforming but can also provide satisfactory performance in terms of flexibility. Although hybrid beamforming is more complex than analog beamforming, the

complexity cost gives the ability to transmit multiple simultaneous beams that can be utilized in mmWave MIMO systems in 5G communications to further increase the data rates.

References

1 Cisco, "Cisco Visual Networking Index: Global Mobile Data Traffic Forecast Update 2015–2020," *Cisco Public Information*, Feb. 2016.

2 NGMN Alliance, " 5G White Paper," 2015. Available at https://www.ngmn.org/uploads/media/NGMN 5G White Paper V1 0.pdf

3 5G PPP, " 5G PPP use cases and performance evaluation models," Version: 1.0, 2016. Available at https://5g-ppp.eu/wp-content/uploads/2014/02/5G-PPP-use-cases-and-performance-evaluation-modeling_v1.0.pdf

4 mmMAGIC, "Use case characterization, KPIs and preferred suitable frequency ranges for future 5G systems between 6 Ghz and 100 Ghz," ICT-671650-mmMAGIC/D1.1, Deliverable D1.1, 2015. Available at https://bscw.5g-mmmagic.eu/pub/bscw.cgi/d54427/mmMAGIC_D1.1.pdf

5 K. Chandra, Z. Cao, T. M. Bruintjes, R. V. Prasad, G. Karagiannis, E. Tangdiongga, H. P. A. van den Boom, and A. B. J. Kokkeler, "mCRAN: A radio access network architecture for 5G indoor communications," in *IEEE ICC 2015 – Workshop on Fiber-Wireless Integrated Technologies, Systems and Networks (ICC'15 – Workshops 09)*, 2015.

6 F. Boccardi, R. W. Heath, Jr., A. Lozano, T. L. Marzetta, and P. Popovski, "Five disruptive technology directions for 5G," *IEEE. Commun. Mag.*, vol. 52, no. 2, pp. 74–80, 2014.

7 K. Chandra, R. V. Prasad, and I. Niemegeers, "An architectural framework for 5G indoor communications," in *IEEE 2015 International Wireless Communications and Mobile Computing Conference (IWCMC)*. 2015, pp. 1144–1149.

8 A. Ghosh, T. A. Thomas, M. C. Cudak, R. Ratasuk, P. Moorut, F. W. Vook, T. S. Rappaport, G. R. MacCartney, S. Sun, and S. Nie, "Millimeter-wave enhanced local area systems: a high-data-rate approach for future wireless networks," *IEEE J. Select. Areas Commun.*, vol. 32, no. 6, pp. 1152–1163, 2014.

9 IEEE Standard for Information Technology, Telecommunications and Information Exchange between Systems Local and Metropolitan Area Networks – Specific Requirements. Part 15.3: Wireless Medium Access Control (MAC) and Physical Layer (PHY) Specifications for High Rate Wireless Personal Area Networks (WPANs) Amendment 2: Millimeter-Wave-Based Alternative Physical Layer Extension, Report, pp. 1–187, Apr. 2009.

10 Standard ECMA-387, High Rate 60 GHz PHY, MAC and HDMI PALs, Dec. 2010.

11 IEEE Standards Association, Draft Standard – Part 11:Wireless LAN Medium Access Control (MAC) and Physical Layer (PHY) Specifications – Amend-

ment 4: Enhancements for Very High Throughput in the 60 GHz Band, IEEE P802.11adTM/D9.0, July 2012.

12 T. Rappaport, S. Sun, R. Mayzus, H. Zhao, Y. Azar, K. Wang, G. Wong, J. Schulz, M. Samimi, and F. Gutierrez, "Millimeter wave mobile communications for 5G cellular: it will work!" *IEEE Access*, vol. 1, pp. 335–349, 2013.

13 C. Dehos, J. Gonzalez, A. De Domenico, D. Ktenas, and L. Dussopt, "Millimeter-wave access and backhauling: the solution to the exponential data traffic increase in 5G mobile communications systems?" *IEEE Commun. Mag.*, vol. 52, no. 9, pp. 88–95, 2014.

14 M. Tercero, P. von Wrycza, A. Amah, J. Widmer, M. Fresia, V. Frascolla, J. Lorca, T. Svensson, M.-H. Hamon, S. Destouet Roblot et al., "5G systems: the mmMAGIC project perspective on use cases and challenges between 6–100 Ghz," in *2016 IEEE Wireless Communications and Networking Conference*, 2016.

15 Flex5Gware, Flexible and efficient hardware/software platforms for 5G network elements and devices, 2015. Available at http://www.flex5gware.eu/

16 A. Osseiran, F. Boccardi, V. Braun, K. Kusume, P. Marsch, M. Maternia, O. Queseth, M. Schellmann, H. Schotten, H. Taoka, H. Tullberg, M. A. Uusitalo, B. Timus, and M. Fallgren, "Scenarios for 5G mobile and wireless communications: the vision of the METIS project," *IEEE Commun. Mag.*, vol. 52, no. 5, pp. 26–35, 2014.

17 W. Roh, J.-Y. Seol, J. Park, B. Lee, J. Lee, Y. Kim, J. Cho, K. Cheun, and F. Aryanfar, "Millimeter-wave beamforming as an enabling technology for 5G cellular communications: theoretical feasibility and prototype results," *IEEE Commun. Mag.*, vol. 52, no. 2, pp. 106–113, 2014.

18 K. Chandra, R. V. Prasad, B. Quang, and I. G. M. M. Niemegeers, "Cog-cell:cognitive interplay between 60 Ghz picocells and 2.4/5 Ghz hotspots in the 5G era," *IEEE Communications Magazine, Special issue on Emerging Applications, Services and Engineering for Cognitive Cellular Systems (EASE4CCS)*, 2015.

19 M. Jacob, S. Priebe, R. Dickhoff, T. Kleine-Ostmann, T. Schrader, and T. Kurner, "Diffraction in mm and sub-mm wave indoor propagation channels," *IEEE Trans. Microw. Theory Tech.*, vol. 60, no. 3, pp. 833–844, 2012.

20 K. Ramachandran, N. Prasad, K. Hosoya, K. Maruhashi, and S. Rangarajan, "Adaptive beamforming for 60 GHz radios: challenges and preliminary solutions," in *Proceedings of the 2010 ACM International Workshop on mmWave Communications: From Circuits to Networks*. ACM, 2010, pp. 33–38.

21 C. Kim, T. Kim, and J.-Y. Seol, "Multi-beam transmission diversity with hybrid beamforming for MIMO-OFDM systems," in *Globecom Workshops (GC Wkshps), 2013 IEEE*. 2013, pp. 61–65.

22 F. Sohrabi and W. Yu, "Hybrid digital and analog beamforming design for large-scale MIMO systems," in *2015 IEEE International Conference on Acoustics, Speech and Signal Processing (ICASSP)*, 2015, pp. 2929–2933.

23 T. L. Marzetta, "Noncooperative cellular wireless with unlimited numbers of base station antennas," *IEEE Trans. Wirel. Commun.*, vol. 9, no. 11, pp. 3590–3600, 2010.

24 O. El Ayach, R. W. Heath, S. Abu-Surra, S. Rajagopal, and Z. Pi, "Low complexity precoding for large millimeter wave MIMO systems," in *2012 IEEE International Conference on Communications (ICC)*, 2012, pp. 3724–3729.

25 O. El Ayach, S. Rajagopal, S. Abu-Surra, Z. Pi, and R. W. Heath, "Spatially sparse precoding in millimeter wave MIMO systems," *IEEE Trans. Wirel. Commun.*, vol. 13, no. 3, pp. 1499–1513, 2014.

26 D. De Donno, J. Palacios, D. Giustiniano, and J. Widmer, "Hybrid analog-digital beam training for mmWave systems with low-resolution RF phase shifters," in *2016 IEEE International Conference on Communications Workshops (ICC)*, 2016.

27 J. Palacios, D. De Donno, and J. Widmer, "Lightweight and effective sector beam pattern synthesis with uniform linear antenna arrays," *IEEE Antennas Wirel. Propag. Lett.*, vol. 16, pp. 605–608, 2016.

28 IEEE Standards Association, IEEE Std 802.15.3c - 2009, Part 15.3: Wireless Medium Access Control (MAC) and Physical Layer (PHY) Specifications for High Rate Wireless Personal Area Networks (WPANs), IEEE Std, 2009.

29 K. Chandra, A. Doff, Z. Cao, R. V. Prasad, and I. Niemegeers, "60 Ghz MAC standardization: progress and way forward," in *2015 12th Annual IEEE Consumer Communications and Networking Conference (CCNC)*, 2015, pp. 182–187.

30 I. C. Society, 802.11ad-2012 – IEEE Standard for Information Technology –Telecommunications and Information Exchange Between Systems – Local and Metropolitan Area Networks – Specific Requirements – Part 11: Wireless LAN Medium Access Control (MAC) and Physical Layer (PHY) Specifications Amendment 3: Enhancements for Very High Throughput in the 60 GHz Band. IEEE, 2012.

31 A. Alkhateeb, O. El Ayach, G. Leus, and R. W. Heath, "Channel estimation and hybrid precoding for millimeter wave cellular systems," *IEEE J. Select. Top. Signal Process.*, vol. 8, no. 5, pp. 831–846, 2014.

32 L. Chen, Y. Yang, X. Chen, and W. Wang, "Multi-stage beamforming codebook for 60GHz WPAN," in *2011 6th International ICST Conference on Communications and Networking in China (CHINACOM)*, 2011, pp. 361–365.

33 T. He and Z. Xiao, "Suboptimal beam search algorithm and codebook design for millimeter-wave communications," *Mob. Netw. Appl.*, vol. 20, no. 1, pp. 86–97, 2015.

34 S. Hur, T. Kim, D. J. Love, J. V. Krogmeier, T. A. Thomas, and A. Ghosh, "Millimeter wave beamforming for wireless backhaul and access in small cell networks," *IEEE Trans. Commun.*, vol. 61, no. 10, pp. 4391–4403, 2013.

35 Z. Xiao, T. He, P. Xia, and X.-G. Xia, "Hierarchical codebook design for beamforming training in millimeter-wave communication," *IEEE Trans. Wirel. Commun.*, vol. 15, no. 5, pp. 3380–3392, 2016.

36 J. Wang, Z. Lan, C.-S. Sum, C.-W. Pyo, J. Gao, T. Baykas, A. Rahman, R. Funada, F. Kojima, I. Lakkis et al., "Beamforming codebook design and performance evaluation for 60GHz wideband WPANs," in *2009 IEEE 70th Vehicular Technology Conference Fall (VTC 2009-Fall)* , 2009, pp. 1–6.

37 W. Zou, Z. Cui, B. Li, Z. Zhou, and Y. Hu, "N-phases based beamforming codebook design scheme for 60 Ghz wireless communication," *J. Beijing Univ. Posts Telecommun.*, vol. 35, no. 3, pp. 1–5, 2012.

38 S. J. Orfanidis, *Electromagnetic Waves and Antennas*. New Brunswick, NJ: Rutgers University, 2002.

39 R. J. Mailloux, *Phased Array Antenna Handbook*, vol. 2. Boston: Artech House, 2005.

40 T. C. Cheston and J. Frank, Phased Array Radar Antennas. *Radar Handbook*, McGraw Hill, 1990, pp. 7–1.

41 D. J. Joaquin, A new low-cost microstrip antenna array for 60 GHz applications, Ph.D. dissertation, Utah State University, 2016.

42 K. Chandra, R. V. Prasad, I. G. M. M. Niemegeers, and A. R. Biswas, "Adaptive beamwidth selection for contention based access periods in millimeter wave WLANS," in *2014 IEEE 11th Consumer Communications and Networking Conference (CCNC)* 2014, pp. 458–464.

43 M. Giordani, M. Mezzavilla, C. N. Barati, S. Rangan, and M. Zorzi, "Comparative analysis of initial access techniques in 5G mmwave cellular networks," in *IEEE 2016 Annual Conference on Information Science and Systems (CISS)*, 2016, pp. 268–273.

Anggrit Dewangkara Yudha Pinangkis is a master's student in electrical engineering at TU Delft. He obtained his bachelor's degree in telecommunication engineering from Institut Teknologi Bandung (ITB) in 2013. From 2013-2014, he was a research assistant at Radio Communication and Microwave Laboratory, ITB. His research interests include antenna beamforming, antenna design, and radar.

Kishor Chandra is a postdoctoral researcher at Delft University of Technology, The Netherlands, where he also received his Ph.D. in 2017. From 2009-2011, he was a research engineer with the Center for Development of Telemetics (CDOT), New Delhi, India, working on IP Multimedia Subsystems. He received his Master of Technology (M.Tech) in signal processing from Indian Institute of Technology (IIT) at Guwahati, India, in 2009 and his Bachelors of Engineering (B.E.) degree in electronics and communications engineering from K.E.C. Dwarahat, India,

in 2007. He is awarded the prestigious Marie Curie Postdoctoral Individual fellowship (MSCA-IF-2017) for a 2-year research stay at CNRS/CentraleSupelec, Paris, France. He is also a recipient of ERCIM Alain Bensoussan Postdoctoral Fellowship. His research interests are in the area of 5G millimeter Wave Communications/Networking and Tactile Internet.

R. Venkatesha Prasad is an assistant professor at the Delft University of Technology, The Netherlands. He received the B.E. degree in electronics and communication engineering and M.Tech. degree in industrial electronics from the University of Mysore, Mysore, India, in 1991 and 1994, respectively, and the Ph.D. degree from the Indian Institute of Science, Bangalore, India, in 2003. He is a distinguished lecturer of IEEE and a senior member of IEEE and ACM.